Magnetization Dynamics of an Individual Single-Crystalline Fe-Filled Carbon Nanotube

Kilian Lenz,* Ryszard Narkowicz, Kai Wagner, Christopher F. Reiche, Julia Körner, Tobias Schneider, Attila Kákay, Helmut Schultheiss, Uhland Weissker, Daniel Wolf, Dieter Suter, Bernd Büchner, Jürgen Fassbender, Thomas Mühl, and Jürgen Lindner

The magnetization dynamics of individual Fe-filled multiwall carbon-nanotubes (FeCNT), grown by chemical vapor deposition, are investigated by microresonator ferromagnetic resonance (FMR) and Brillouin light scattering (BLS) microscopy and corroborated by micromagnetic simulations. Currently, only static magnetometry measurements are available. They suggest that the FeCNTs consist of a single-crystalline Fe nanowire throughout the length. The number and structure of the FMR lines and the abrupt decay of the spin-wave transport seen in BLS indicate, however, that the Fe filling is not a single straight piece along the length. Therefore, a stepwise cutting procedure is applied in order to investigate the evolution of the ferromagnetic resonance lines as a function of the nanowire length. The results show that the FeCNT is indeed not homogeneous along the full length but is built from 300 to 400 nm long single-crystalline segments. These segments consist of magnetically high quality Fe nanowires with almost the bulk values of Fe and with a similar small damping in relation to thin films, promoting FeCNTs as appealing candidates for spin-wave transport in magnonic applications.

1. Introduction

Recent progress in material science has allowed the production of exciting materials, such as rolled-up and flexible magnetic nanomembranes,[1,2] shapeable nanoelectronics,[3] circular nanowires and nanotubes and even printable spintronic devices.[4] The fabrication of nanowires and nanotubes[5,6] is motivated by a broad range of applications for magnetoresistive devices, optical meta-materials, cell-DNA separators, drug delivery vectors,[7,8] and wave based information transport.[9] Both, the high stability of their magnetic equilibrium state against external perturbations, as well as their robust domain walls, which propagate with velocities faster than the spin wave phase velocity, promote them as appealing candidates for racetrack memory devices and for information transport and processing using spin waves in magnonic applications.

Various bottom-up synthesis routes for the preparation of magnetic nanowires exist; including for example electro-deposition based on porous membrane templates[1] and pyrolysis of metal–organic precursors. In particular the pyrolysis of ferrocene allows for the formation of iron-filled carbon nanotubes (FeCNT), i.e., multiwall carbon nanotubes, which contain single-phase single-crystalline iron nanowires,[10–14] where the body-centered cubic iron phase dominates. Furthermore, iron nanowires with various crystal orientations can be found with no prevalent orientation.[13] The diameters of the carbon nanotubes and the embedded iron nanowires are in the range of 30–100 and 10–40 nm, respectively.[13]

Dr. K. Lenz, Dr. R. Narkowicz, Dr. K. Wagner, Dr. T. Schneider,
Dr. A. Kákay, Dr. H. Schultheiss, Prof. J. Fassbender, Dr. J. Lindner
Helmholtz-Zentrum Dresden – Rossendorf
Institute of Ion Beam Physics and Materials Research
Bautzner Landstr. 400, 01328 Dresden, Germany
E-mail: k.lenz@hzdr.de
Dr. C. F. Reiche, Dr. J. Körner, Dr. U. Weissker, Dr. D. Wolf,
Prof. B. Büchner, Dr. T. Mühl
Leibniz Institute for Solid State and Materials Research
IFW Dresden
Helmholtzstr. 20, 01069 Dresden, Germany

Dr. T. Schneider
Technische Universität Chemnitz
Institute of Physics
Reichenhainer Str. 70, 09107 Chemnitz, Germany
Dr. H. Schultheiss, Prof. B. Büchner, Prof. J. Fassbender
Institute for Physics of Solids
Technische Universität Dresden
Zellescher Weg 16, 01069 Dresden, Germany
Dr. U. Weissker
Transfer Office
Technische Universität Dresden
Helmholtzstr. 9, 01069 Dresden, Germany
Prof. D. Suter
Department of Physics
Technical University of Dortmund
Otto-Hahn-Straße 4a, 44227 Dortmund, Germany
Prof. B. Büchner, Dr. T. Mühl
Center for Transport and Devices of Emergent Materials
Technische Universität Dresden
01062 Dresden, Germany

**ADVANCED
SCIENCE NEWS**

www.advancedsciencenews.com

**NANO · MICRO
small**

www.small-journal.com

The magnetic configuration and magnetization reversal of individual FeCNTs have been studied by employing various nanomagnetometries, like Hall effect measurements,[15] cantilever-based approaches,[16,17] and superconducting quantum interference device (SQUID) magnetometry[18] as well as magnetic force microscopy (MFM).[19] It was found that the spontaneous and the remanent magnetization of FeCNTs are always in a single domain state and oriented along its long axis. When applying external fields along the easy axis, switching fields between 100 and 400 mT are observed. The thermally assisted magnetization reversal of FeCNTs is dominated by the nucleation of a small reversed domain via curling and subsequent fast propagation of a domain wall, resulting in a reversed single domain state.[15,16] The high stability of their magnetic equilibrium state together with their superior mechanical properties provided by the carbon nanotube, promotes FeCNTs to be used as probes for quantitative magnetic force microscopy.[20,21] As reported, sophisticated FeCNT probes for simultaneous perpendicular and in-plane MFM sensitivity were also developed.[22,23]

Up to now, experiments have focused on investigating the static magnetic properties of these FeCNTs. These experimental results suggest that the Fe filling is magnetically homogeneous throughout the CNT, i.e., with no measureable variation of the material properties from the magnetostatic point of view. In contrast to that, our study on the magnetization dynamics reveals a different scenario. We present clear indications by analysis of the ferromagnetic resonance (FMR) lines[24–26] and the abrupt decay of the spin-wave transport seen in the spatially resolved Brillouin light scattering (BLS)[27] measurements that the Fe filling is not a homogeneous single crystal whisker throughout the nanowire. A stepwise cut and measurement procedure was applied in order to investigate the evolution of the ferromagnetic resonance lines as a function of the nanowire length. Our results show that the FeCNT is indeed not homogeneous but is built from 300 to 400 nm long single-crystalline segments.

Based on the experimental results together with micromagnetic simulations, it can be concluded that each of these segments is a magnetically high quality Fe nanowire with almost the bulk properties of Fe.[28] The single-crystal aspect together with the very small linewidth obtained from measurements promotes the FeCNTs as appealing candidates for spin-wave transport in magnonic applications.

2. Experimental Details

The FeCNTs have been prepared by chemical vapor deposition in a two-zone furnace. Ferrocene $(C_5H_5)_2Fe$, an organometallic powder precursor compound, is sublimated in the first reactor zone at 150 °C and then forwarded under a constant flow of argon to the second zone, i.e., the reaction zone of the furnace. There, the Si substrate, having a 10 nm Al buffer layer and a 2 nm Fe seed layer on top, is placed. To initiate the ferrocene pyrolysis and the FeCNT formation, the temperature within the reaction zone is increased from 300 to 800 °C at a rate of 0.6 K s^{-1}. This leads to the growth of FeCNTs with a long, continuous, high aspect ratio iron nanowire filling. Further details of the process can be found elsewhere.[29–32]

Single FeCNTs are picked up from the substrate by micromanipulation (see **Figure 1**a) within a dual beam system, i.e., a combined scanning electron microscope (SEM) and focused ion beam (FIB) system. They are transferred either into the microresonator loops for FMR measurements (see the example in Figure 1b and the final sample in Figure 5a), or onto a substrate with a microwave antenna for the BLS measurements. Further details can be found in the Experimental Section.

Figure 1c–e shows transmission electron microscopy (TEM) images of typical FeCNT. The dark material contrast in Figure 1c depicts the 35-nm-diameter Fe filling inside the multiwall CNT. There are only a few defects, slight kinks, and
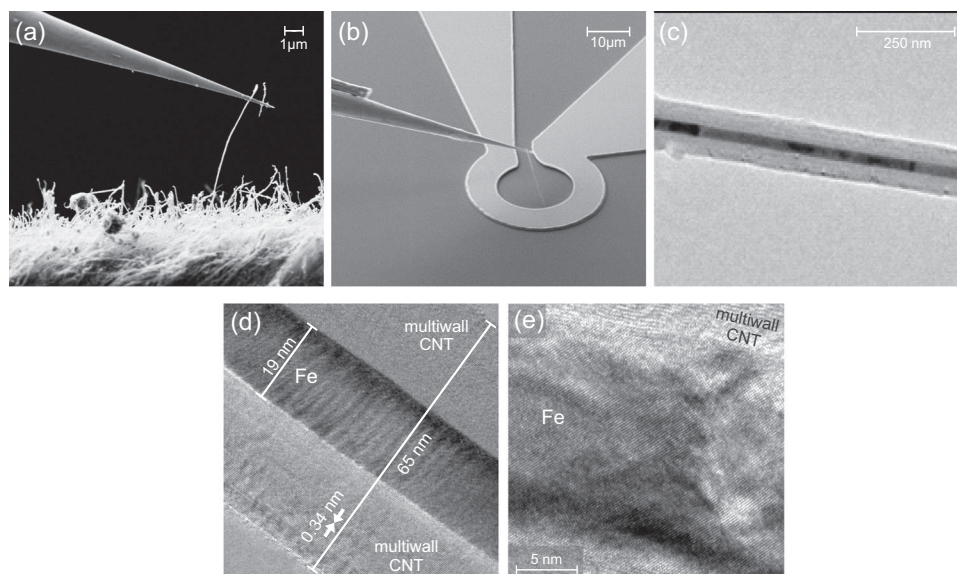

Figure 1. a) Pickup of a single FeCNT and b) placement into the microresonator using a micromanipulator with a tungsten tip imaged by SEM. c) TEM image of a typical FeCNT showing the multiwall CNT (grey) around the Fe filling (dark) with only a few defects. d,e) High-resolution TEM images resolving the single-crystalline bcc-Fe filling and the CNT wall spacing.

**ADVANCED
SCIENCE NEWS**

www.advancedsciencenews.com

NANO · MICRO

small

www.small-journal.com

Table 1. Dimensions (Fe filling only) of investigated FeCNT samples. Suffixes of FeCNT#2 denote the different cutting steps.

FeCNT-	Length [µm]	Diameter [nm]
#1	14.5	20
#2-pristine	12.2	41
#2-cut1	9.6	41
#2-cut2	4.2	41
#2-cut3	2.2	41
#4	0.73	21

thickness variations visible. The high-resolution TEM images Figure 1d,e of another FeCNT reveal the single-crystalline character of the body-centered cubic (bcc) Fe filling.

Table 1 lists the experimentally investigated FeCNTs. All FeCNTs were processed under the same conditions using the same substrate. As described later, FeCNT#2 was successively measured by FMR and trimmed to shorter lengths. Note, that in the following the dimensions given for the FeCNTs denote the length and diameter of the Fe filling only.

3. Results and Discussion

Both, FMR and BLS measurements could be theoretically predicted if the FeCNT filling would be a single crystalline nanowire. The spatially resolved thermal spectra of the BLS measurements should show well-defined frequency excitations or magnon modes homogeneously distributed along the nanowire length. The FMR measurements, concerning the frequency versus field dependence and the angular evolution of the resonance fields shown in **Figure 2** can be calculated using the equations formulated in the Experimental Section.

The resonance fields are calculated analytically assuming a cylindrical Fe nanowire with 10 µm length, 41 nm diameter, and Fe-bulk properties[28] that are—saturation magnetization $M_s = 1710$ kA m^{-1}, cubic magnetocrystalline anisotropy field $K_4/M_s = 28.05$ mT, Landé g-factor $g = 2.09$. As seen from Figure 2a, the zero-field resonance frequency is about 33 GHz. When the external magnetic field is applied along the long (easy) axis of the nanowire (i.e., $\theta_H = 0°$) the resonance frequency increases with increasing magnetic fields (green curve). Since we use microresonators with a resonance frequency close to 14 GHz (dashed line), no resonance line would be observable. If the external field is aligned perpendicular to the long axis, (i.e., $\theta_H = 90°$), two resonances are present for frequencies below 33 GHz (blue and red curve) and one resonance above (red curve). These are the so-called unaligned and aligned modes of the uniform precession. The angular dependence of the resonance field for a fixed frequency (14.65 GHz) is depicted in Figure 2b. According to the theoretical description, the two resonances (blue and red curve) are observable only within a narrow angular range of ± 2° around the 90° direction. In the following we will compare the BLS as well as the FMR measurement results with these expectations.

Figure 3a shows a scan of the thermal spin-wave spectrum along the 14.5-µm-long FeCNT#1 measured by microfocus Brillouin light scattering (µBLS). Red color denotes a high BLS intensity, blue a low intensity. For the BLS measurements the FeCNT was placed by micromanipulation on a Si substrate with a simple coplanar microwave antenna patterned previously. The thermal spectrum was collected in a static magnetic field of 800 mT applied perpendicular to the long axis of the FeCNT. The detected resonances, consisting at least of two peaks, vary between 22 and 27 GHz along the FeCNT. As the frequencies and intensities of the BLS peaks are not constant this obviously indicates that the internal field directly related to the magnetic properties is changing over the length of the FeCNT piece. This is further supported by the abrupt decay of the intensity at certain positions. For example the intensity-drop around the position at 0.3 µm might be due to a nonmagnetic gap in the FeCNT. This could be a geometrical gap or just degraded magnetization at this point. The lower frequencies around 0.4 µm might be due to a kink at this position, which results in a slightly different field angle. The constant signal over the length at 34.5 GHz is attributed to a phonon mode of the substrate (see Figure 3b).

Figure 4a shows microresonator FMR spectra taken of the FeCNT#2-pristine within the small accessible frequency range around 13 GHz with the magnetic field applied perpendicular to the long axis, i.e., $\theta_H = 90°$. Several resonances are visible for each frequency. The resonances below $\mu_0H = 1$ T move to lower
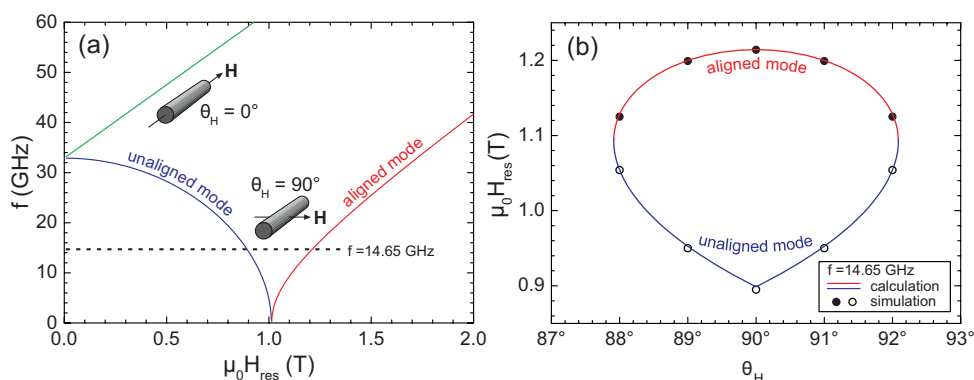

Figure 2. a) Calculated FMR frequency-field dependence of a 10-µm-long, 41 nm diameter Fe cylinder with the external field aligned along the long axis (green curve) and perpendicular to it (blue/red curves). b) Angular dependence of the same cylinder around the perpendicular direction. Two resonance branches are visible. Circles denote results from micromagnetic simulations.
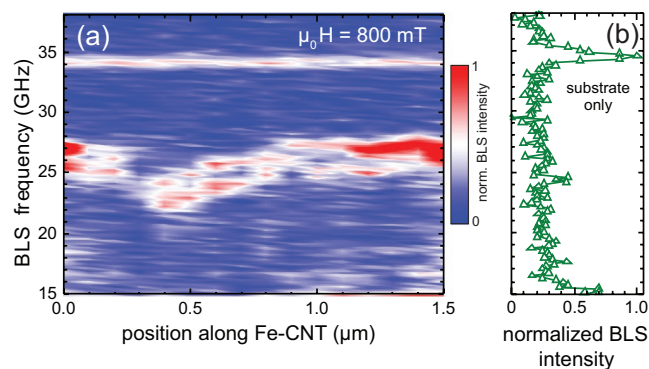
**ADVANCED
SCIENCE NEWS**

www.advancedsciencenews.com

NANO · MICRO

small

www.small-journal.com

Figure 3. a) Variation of the thermal spin-wave spectrum along a section of the 14.5-µm-long FeCNT#1 recorded by µBLS. A field of 800 mT was applied perpendicular to the FeCNT. Red color denotes a high BLS intensity. b) BLS background spectrum recorded on the substrate. The signal peak having a constant frequency of 34.5 GHz and clearly being independent from the measurement position in panel (a), can be attributed to a phonon mode of the silicon substrate.

fields with increasing frequency, whereas the modes above move to higher resonance fields as highlighted by the grey hatched areas, respectively. This means that the lower modes can be attributed to the so-called unaligned modes, i.e., the external field is not yet strong enough to pull the magnetization in its direction. Therefore, the internal magnetic fields determine the axis of precession. In contrast, the modes at higher fields are the aligned modes processing around the external field's axis.

Figure 4b shows the spin-wave intensity measured by µBLS using external microwave excitation. For this the 14.5 µm long and 20 nm diameter FeCNT#1 was placed on a substrate close to a lithographically prepared microwave antenna. This allows for broadband measurements and especially higher frequencies in contrast to the fixed-frequency measurements using the microresonator. The spectra were recorded for various magnetic fields between 0 mT (black curve) and 800 mT (yellow curve) applied at an angle of $\theta_H = 85°$. With increasing field strength the peaks shift to lower frequencies. Hence, these are unaligned modes. Like for the FMR measurement each

spectrum consists of several peaks mainly left of the highest peak. Figure 4c shows the resonance fields of the FMR and BLS data together with fits (solid lines) calculated from the resonance equation (see Experimental Section) considering demagnetizing factors according to the shape and dimensions of the FeCNTs as given in **Table 1**. The horizontal and vertical offsets between the FMR and BLS data (blue and black/red curves) are attributed to the changing demagnetizing factors, i.e., due to the different lengths.

To elucidate the origin of the multiple peaks seen in the FMR and BLS spectra of Figure 4a,b a systematic angle-dependent microresonator FMR study was performed.

Figure 5a shows a SEM image of the ≈12.2 µm long, 41 nm diameter FeCNT#2-pristine placed inside a microresonator. The FeCNT is fixed to the substrate by carbon depositions visible as small hillocks. Due to the placement by micromanipulation, the FeCNT is slightly distorted. The white dashed lines mark segments of the FeCNT, which show different rotation angles. The angles are given with respect to the middle segment labeled "0°". The yellow lines illustrate the segments. The coordinate system depicts the field angle for the FMR measurements. As before, the external field is applied perpendicular to the long axis of the FeCNT when $\theta_H = 90°$. Figure 5e shows the corresponding in-plane angular dependence of the resonance fields as detected by the microresonator FMR. The resonance fields have been determined from Lorentzian fits to the FMR spectra. For clarity only resonances above 1.0 T are displayed, i.e., the aligned modes. One can see a multitude of resonances per angle, which resembles a superposition of several parabola-like arcs. By comparison to the angular dependence in Figure 2b matching the red curve, it is obvious that these parabolas represent the aligned uniform resonance modes. The center of the parabola would denote the hard axis of the nanowire, i.e., the direction perpendicular to the long axis.

In the next step a short part of the right-hand side of the FeCNT#2-pristine was removed by a focused Ga ion beam (as described in the Experimental Section), resulting in the geometry depicted in Figure 5b. The green box denotes the rest of it, named FeCNT#2-cut1, which was measured again by FMR. The corresponding FMR data in Figure 5f clearly shows that the previous resonances around 93°–97° (grey circles) have
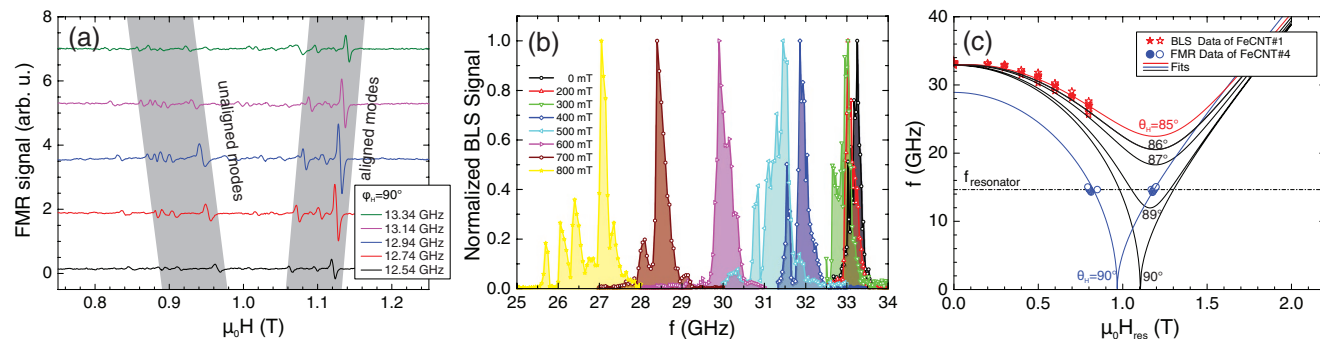

Figure 4. a) FMR spectra of the 12.2-µm-long FeCNT#2-pristine at various frequencies with the field applied perpendicular to the long axis, i.e., $\theta_H = 90°$. The hatched areas are guides to the eye showing the resonance field shift with frequency. b) Efficiency of the spin-wave excitation of the 14.5-µm-long FeCNT#1 as a function of excitation frequency for different magnetic fields applied close to the short axis ($\theta_H = 85°$). The spin-wave intensity has been recorded by µBLS close to the microwave antenna and normalized to its maximum value. c) Resonance conditions as determined by FMR (blue circles, 730 nm short FeCNT#4) and µBLS (red stars, peaks from panel (b)) together with corresponding resonance equation fit (solid lines).
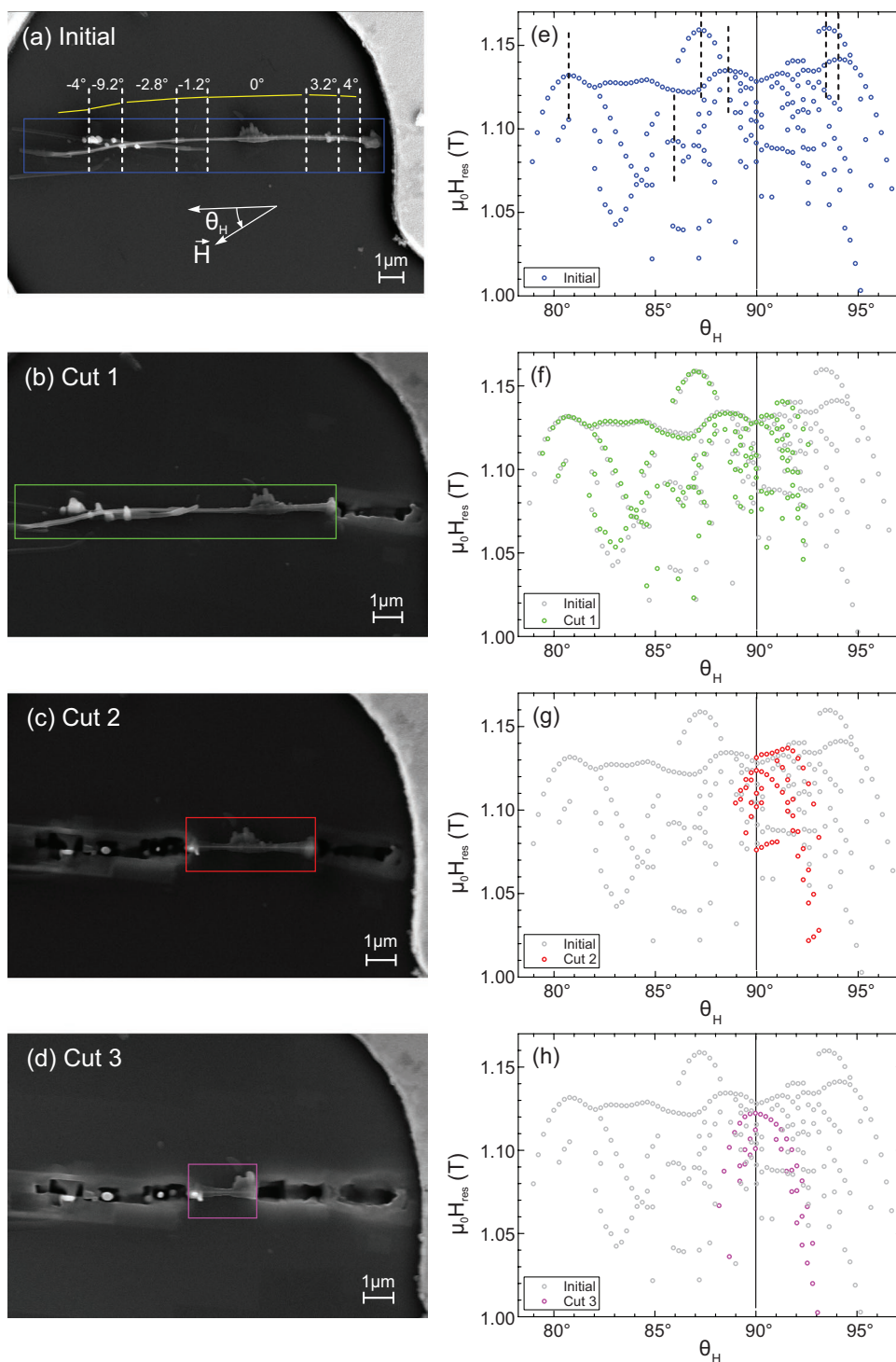
Figure 5. SEM images of the FeCNT#2 inside the microresonator a) before and b–d) after successive FIB cuts. The remaining FeCNT pieces are marked by boxes. e–h) Corresponding angle-dependent FMR measurements taken after each cut. Dashed white lines and solid yellow lines in inset (a) illustrate rotated segments of the FeCNT. Rotation angles are relative to the middle segment at 0° (corresponding to resonances at $\theta_H = 90°$). Grey circles repeat the initial data from inset (e). Dimensions are given in Table 1.

vanished. Therefore, they can be attributed to the part, which was removed. For the second FIB cut shown in Figure 5c most of the wrinkled and misaligned left-hand side of the FeCNT#2-cut1 was removed. Subsequently the FMR angular dependence

was measured again and is shown in Figure 5g as FeCNT#2-cut2. The result is now much simpler, as it contains only up to four modes per angle, located around 89°–93°. This angular dependence is already quite close to what one would expect

from a straight nanowire according to the theory. The angular shift of the resonance curves also matches the kink-angles between the segments of the FeCNT#2-pristine (left part: −9.2° and −4°, right end: +4°) visible in the SEM images. Finally, the third FIB cut left the 2.15 µm short piece FeCNT#2-cut3 for measurement, which shows only two parabolas slightly offset to each other. This means that this residual 2 µm long piece seems to consist of two straight parts only, enclosing an angle of less than a degree between their long axis. Alternatively, the two parts may have different magneto-crystalline easy axes orientation. Finally the rest of the sample was removed by FIB to check, whether there are residual signals from the substrate, which was not the case. There was only a weak paramagnetic signal (i.e., g-factor $g = 2$) proving the sufficient sensitivity for detection.

It has been reported previously that the crystallographic structure of the Fe-filling inside a free standing FeCNT—although being of quite good quality overall—exhibits segments of various lattice planes on short length scales 14. This matches the FMR and BLS findings that the FeCNTs under investigation consist of at least two or more segments. This might be inherent to the growth of the FeCNTs and on the micrometer scale caused by the micromanipulation and placement on the substrate, which shows bends and wrinkles of a few degrees as can be seen from Figure 5a.

To determine the magnetocrystalline anisotropy and damping of the FeCNT, special care has been taken to find a straight piece of FeCNT. After selecting a few straight FeCNTs they were mounted with one end to a TEM grid and inspected at high magnification. From this inspection straight sections have been determined. Then such a section was cut out and transferred into the microresonator taking care not to bend and stress the FeCNT while mounting it by carbon depositions. The result is the 730-nm-long FeCNT#4 piece with a core diameter of 21 nm.

Figure 6a shows the measured resonance fields as a function of the in-plane angle. Resonances can be observed only within a small angular range of ±3° around the hard axis. The results clearly suggest that even the 730-nm-FeCNT#4 piece consists of two segments with different intrinsic material properties, such as the alignment of the magnetocrystalline anisotropy direction with respect to the long axis of the nanowire.

The following approach was used to determine their length: the integral of the FMR absorption line is proportional to the amount of magnetic material involved. Hence, the ratio of the integrals of the main peaks is proportional to the length ratio of the two sections. From the overall length of 730 nm it follows that the two pieces have a length of ≈240 and 490 nm, respectively, with an uncertainty of about 30 nm.

To obtain a deeper insight into the influences the presumably multiple segments with their different magnetocrystalline anisotropy axes orientation have on the FMR spectra, micromagnetic simulations have been performed. This is needed since the analytical model described at the beginning of the manuscript cannot properly account for the rotation of the cubic anisotropy axes with respect to the cylinder axis. We have performed micromagnetic simulations of the FMR spectra (for details see the Experimental Section) of a 730-nm-long FeCNT consisting of two sections with 490 and 240 nm length

at integer θ_H angles between 87° and 93° at the same resonance frequency used in the experiments. Fe bulk properties ($Ms = 1710$ kA m^{-1}, exchange stiffness $A = 2.1$ pJ m^{-1} and cubic anisotropy $K_4 = 46.8$ kJ m^{-3}) have been used. Note that the micromagnetic simulations of the FeCNTs are computational demanding and therefore time consuming. Hence they cannot be used as a fitting procedure to determine the anisotropy for example. Nevertheless one can compare the simulations with the experimental findings.

To achieve the skew observed in the aligned modes, the (001) crystallographic plane was tilted with respect to the geometrical long axis by +2° for the short and by −1° for the long segment, respectively. The obtained results are depicted in Figure 6b,d. It can be seen that the aligned mode (red circles) at fields when the magnetization is saturated perpendicular to the long axis ($\theta_H = 90°$) is similar to that shown in Figure 2b based on analytical considerations. However, in the experimental results of Figure 6a one can identify *two* segments of aligned modes (red circles), which might even look shifted by 0.4° with respect to each other. The simulation of a single wire with two lattice planes only shows *one* aligned mode, because the shape anisotropy is the dominating quantity in the system, not the cubic anisotropy. Moreover, the skew is not visible. The large separation of the resonance modes depicted by the blue circles and squares is also contradictory to the experimental results. The corresponding map of the m_z-component of the resonance modes (at $\theta_H = 90°$ and $f = 14.6575$ GHz) in Figure 6d shows that the mode given by the blue circles is the unaligned mode and the mode depicted by the blue squares is an edge mode, i.e., a resonant mode where the resonance is localized only at the very ends of the FeCNT. Altogether, a tilt of the crystallographic planes of the different sections alone—even with different angles—cannot account for the asymmetry observed in the experimental data.

As a further step, a 20 nm nonmagnetic gap has been introduced between the 490 and the 240 nm segments while keeping all the material parameters and the lattice tilts the same like in Figure 6b. Note that geometrical gaps (no material) have not been found in the TEM imaging during preparation. Hence, the Fe filling might be magnetically dead or degraded in this gap. The resonances are plotted in Figure 6c and the maps in Figure 6e. By introducing this 20 nm gap between the two pieces, two sections of aligned modes appear (red semifilled circles), similar to the experimental data. The excitation maps in Figure 6e show that each segment has its own aligned mode, while the other segment is not excited. This time the strong shape anisotropy is reduced due to the segmentation. Thus, the cubic anisotropy of the two segments with their slightly different lattice planes becomes visible in the skew of the angular dependence of the aligned modes—The two sections approach each other or intersect at angles above 92°. If one carefully looks at the experimental spectrum, similarly two segments can be seen in Figure 6a with a crossing of the resonances around 91.3°. Note, the unaligned and edge mode (blue symbols) now also show more similarities to the experimental data. Although the simulation does not match the experimental data perfectly, we conclude that the 730-nm-long FeCNT#4 piece measured experimentally consists of two pieces with different crystallographic orientation but separated by a short nonmagnetic gap.
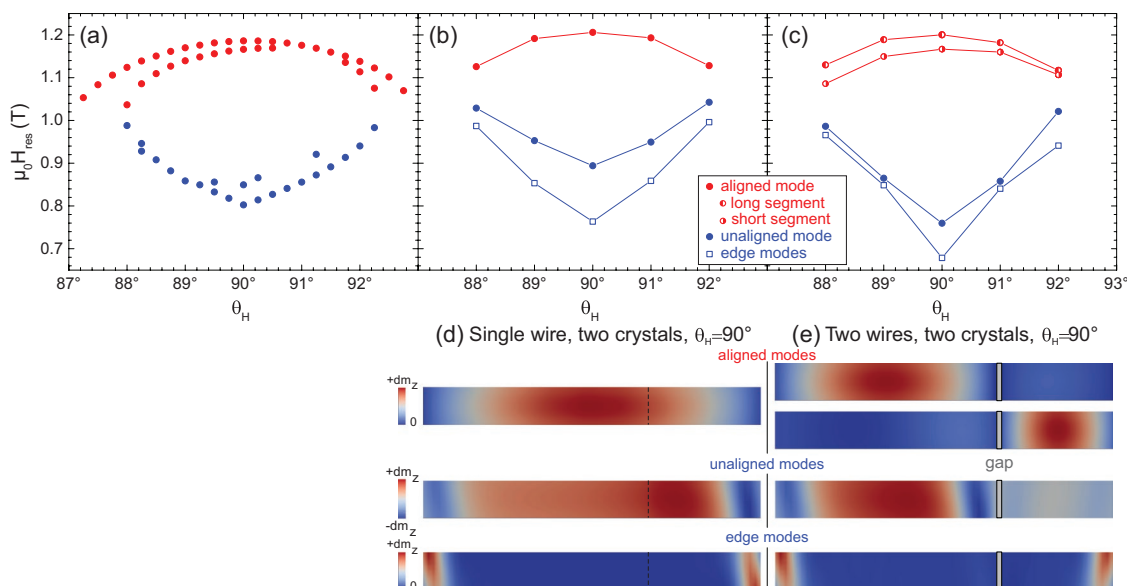
Figure 6. Angular dependence of the 730-nm-long sample FeCNT#4 at $f = 14.6575$ GHz obtained from a) experiment and b,c) simulations. The experimental data from inset (a) suggests that the FeCNT#4 should consist of two segments. b) Simulated resonance fields of the 730 nm long FeCNT#4 with two sections of different orientations of the cubic anisotropy (marked by dashed line in inset (d): a 490 nm section with $-1°$ and a 240 nm section with $+2°$ misalignment with respect to the long axis. d) Solid red circles denote the aligned mode, blue circles the unaligned mode, and blue open squares the edge mode as depicted. c) Same segments and angles as in inset (b) but separated by a 20 nm gap between the individual sections. e) Red circles denote the aligned modes of the individual segments as depicted. Solid lines are guides to the eye. d,e) Snapshots of the m_z-component of the resonant modes at $\theta_H = 90°$.

This conclusion is also in coherence with the observed abrupt decay of the spin-wave intensity in BLS measurements.

Finally it is worthwhile to take a look at the resonance linewidth of the FeCNT. **Figure 7** shows the FMR spectrum of the 730 nm long sample FeCNT#4 measured at $\theta_H = 90°$ and $f = 14.6575$ GHz. There are four clearly visible resonances. The red curves are Lorentzian fits illustrating the narrow linewidths of around 4 mT. This linewidth is half that of Fe whiskers (Fe microwires with 30–90 μm rectangular cross-section and millimeter length)[33] and in the same range as epitaxial

≈20 nm thick Fe films on GaAs(110)[34,35] and GaAs(001)[36] or MgO(001).[37] This result is of particular interest because it shows that although the FeCNT nanowires consist of multiple crystallites, the quality of the individual crystallite sections must be very high. The narrow linewidth indicates that line broadening due to sample imperfections and inhomogeneity seems to be negligible.

4. Conclusion

Single Fe-filled carbon nanotubes have been investigated by microresonator ferromagnetic resonance and microfocused Brillouin light scattering experiments. The experimental results in combination with micromagnetic simulations show that the longer FeCNTs consist of several segments, each having Fe-bulk like magnetic properties. The FeCNTs have been successively trimmed by FIB to obtain almost single-crystalline pieces. The measurements reveal that even the 730-nm-short FeCNT#4 piece consists of two segments with a slight variation of the c-axis orientations and presumably a short gap in between. The visible resonances at higher fields are the aligned modes of the segments. At lower fields there exists an unaligned mode in the longer segment and the edge mode at the ends of the FeCNT. The small linewidths of the FMR spectra indicate that the individual Fe segments must be of a very high quality, single crystalline Fe with negligible sample imperfections and inhomogeneity of the material parameters. We believe that the single crystal nature as well as the small linewidth measured in this study (suggesting small damping) are promoting FeCNTs as appealing candidates for spin-wave transport in magnonic applications.
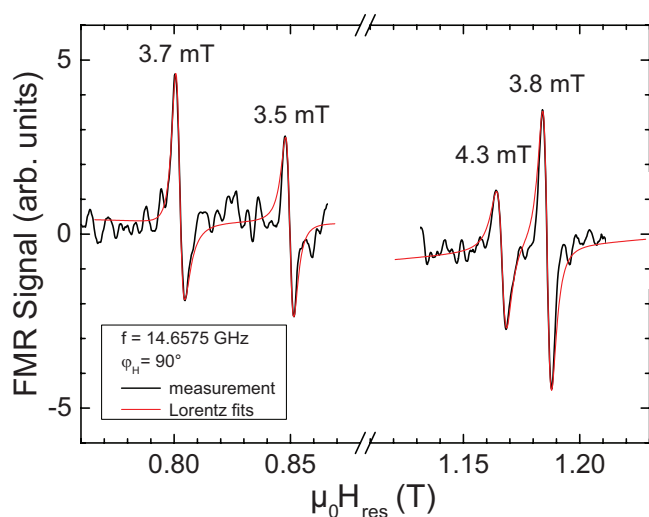

Figure 7. Spectrum of the 730 nm long FeCNT#4 (black) and Lorentzian fits (red) at $\theta_H = 90°$. Numbers denote the linewidths $\mu_0 \Delta H_{pp}$ of the resonances.

**ADVANCED
SCIENCE NEWS**

www.advancedsciencenews.com

**NANO · MICRO
small**

www.small-journal.com

5. Experimental Section

Micromanipulation of FeCNT: For the placement of the FeCNT into the loop of the planar microresonator a combined FIB–SEM instrument (1540XB CrossBeam, Carl Zeiss AG) that includes a gas injection system (GIS) and a micromanipulator (MM3A-EM with ROTIP-EM, Kleindiek Nanotechnik GmbH) was used. The latter was equipped with an etched tungsten needle as a manipulation tool. The CVD created FeCNTs grow in an aligned carpet-like fashion on their substrate (see Figure 1a). After transfer to the FIB–SEM system the micromanipulator was employed to bring the tungsten needle tip in contact with the free end of an FeCNT using the SEM mode of the system. Subsequently, a carbon containing precursor gas was injected in the vicinity of the needle tip via the GIS to glue the FeCNT to the tungsten needle by electron beam induced deposition of amorphous carbon. It is important to keep the deposition time brief, so the bond between the FeCNT and the needle tip is durable enough to survive the following manipulation steps but not too strong to prevent releasing it after the FeCNT is attached to the microresonator substrate. To mount the FeCNT to the microresonator, the sample has to be nearly parallel to the image plane and aligned with the direction of the opening of the micro coils with the stage positioned considerably lower than the needle (see Figure 1b). After tilting the sample stage by about 20°, the stage is carefully raised until the protruding FeCNT end almost touches the substrate. Then the FeCNT nanotube was carefully threaded into the resonator loop. The free end was glued to the substrate by carbon deposition—this time with a longer duration and wider area to create a solid bond. By pulling the needle away from the substrate along the direction of the carbon nanotube, the bond between the needle and FeCNT was broken. Then the needle is used to push down the nanotube end. By squeezing it to the substrate while carefully moving the needle, the FeCNT is slightly stretched to further achieve a more parallel orientation of the Fe nanowire with respect to the substrate. Finally the FeCNT was fixed in this state again by amorphous carbon deposition. The diameter of the carbon nanotube's Fe filling was examined using the material contrast between Fe core and the carbon shell in the electron beam image.

In order to shorten the FeCNT nanowire after each FMR angle-series, the Ga FIB functionality of the equipment was used. Great care was taken in this step to not irradiate parts of the FeCNT that were later used for magnetic measurements: The FIB was targeted in reduced area imaging mode close to the part of the carbon nanotube to be removed. The reduced ion beam scanning area was then moved in small steps over the FeCNT portion to be removed. Any part that was irradiated once was completely removed, along with a larger portion of the substrate surface for complete removal of the magnetic material. It was found in previous experiments that a FeCNT that was cut with a FIB in this way very quickly loses its ferromagnetic properties, possibly due to oxidation of the exposed Fe core ends. Thus, the open ends were closed by carbon depositions using the GIS. The observed long term stability of the sample's ferromagnetic signal during the experiments demonstrates the viability of this approach.

TEM: The structure of the FeCNTs at nanometer and atomic resolution was characterized using an FEI Tecnai F30 TEM instrument

(ThermoFisher Scientific Company, USA) operated at an acceleration voltage of 300 kV.

Microresonator FMR: The microresonator loop was needed for achieving the necessary ultrahigh-sensitivity within the ferromagnetic resonance investigation. As described[24–26,38] the microresonator loop with its tuning elements (not shown in Figure 1b) made up a resonant circuit tuned to an impedance of 50 Ω and a resonance frequency around 14 GHz. The key to achieve the high sensitivity necessary to measure FMR of single nano-objects was the tremendous increase of the resonator's filling factor. Currently, the microresonator FMR is capable of detecting signals from just roughly 10^6 atoms, which is orders of magnitude better than using a conventional x-band cavity for example, where ≈10^{11} spins are necessary. With respect to the lengths of the FeCNTs, an inner loop diameter of 20 μm was selected to maximize the filling factor. The microresonator was connected via a circulator to a home-built microwave spectrometer, working in reflection mode at the resonator's design frequency of around 14 GHz. The derivatives of the FMR absorption and dispersion with respect to the external field were recorded using field modulation and lock-in technique while sweeping the external magnetic field.

μBLS: The spin-wave intensity was measured locally by means of micro-focused Brillouin light spectroscopy[27] at room temperature. Light from a continuous-wave, single-frequency 532 nm solid-state laser was focused to a laser spot and scanned over the Fe-filled carbon nanotube. The back-scattered light was then analyzed using a six-pass Fabry–Perot interferometer TFP-2 (JRS Scientific Instruments) and the BLS intensity is proportional to the square of the amplitude of the magnetization dynamics at the laser spot position. For the conditions of the presented measurements the spectral and spatial resolution full width at half maximum (FWHM) was experimentally determined to be ≈190 ± 30 MHz and ≈340 ± 50 nm, respectively.

Magnetic Anisotropy Energy: The fit curves to the FMR data are calculated using Baselgia's formalism to derive the resonance equation from the free energy density of the system.[39] Considering the macrospin model the free energy density for a cubic (001) system including demagnetizing factors reads

$$F = -\mu_0 \vec{M} \cdot \vec{H} + \left(-\frac{1}{2}N_z\mu_0 M_s^2 + K_{2\perp} + \frac{1}{2}N_x\mu_0 M_s^2\cos^2\varphi + \frac{1}{2}N_y\mu_0 M_s^2\sin^2\varphi\right)\sin^2\theta$$
$$-\frac{K_4}{2}\cos^4\theta - \frac{K_4}{8}(3+\cos4\varphi)\sin^4\theta \tag{1}$$

where M and H are the magnetization and external magnetic field, respectively. N_x, N_z, and N_y are the demagnetizing factors. They have to be calculated according to the geometry of the object.[40,41] $\mu_0 M_s$ is the saturation magnetization, φ and θ are the spherical magnetization angles. K_4 is the cubic magnetocrystalline anisotropy constant and $K_{2\perp}$ is the uniaxial out-of-plane anisotropy, respectively. The equilibrium angles of the magnetization for a given set of parameters are determined by minimizing the derivative of Equation (1) with respect to the corresponding angle. Inserting F and its derivatives into Baselgia's general resonance equation[39] yields

$$\left(\frac{\omega}{\gamma}\right)^2 = \left\{\mu_0 H_0\left[\sin\theta\sin\theta_H\cos(\varphi-\varphi_H)+\cos\theta\cos\theta_H\right]+\left(-\mu_0 M_s N_z+\frac{2K_{2\perp}}{M_s}-\mu_0 M_s\left(N_x\cos^2\varphi+N_y\sin^2\varphi\right)+\frac{K_4}{M_s}-\frac{K_4}{M_s}[3+\cos4\varphi]\right)\cos2\theta+\left(\frac{K_4}{M_s}+\frac{K_4}{4M_s}[3+\cos4\varphi]\right)\cos4\theta\right\}$$
$$\times\left\{\mu_0 H_0\left[\sin\theta\sin\theta_H\cos(\varphi-\varphi_H)+\cos\theta\cos\theta_H\right]+\left(-\mu_0 M_s N_z+\frac{2K_{2\perp}}{M_s}-\mu_0 M_s\left(N_x\cos^2\varphi+N_y\sin^2\varphi\right)-\frac{K_4}{2M_s}[3+5\cos4\varphi]\right)\cos^2\theta+\left(\frac{2K_4}{M_s}+\frac{K_4}{2M_s}[3+\cos4\varphi]\right)\cos^4\theta+\frac{2K_4}{M_s}\cos4\varphi+\mu_0 M_s\left(N_y-N_x\right)\cos2\varphi\right\}$$
$$-\left\{\left[\frac{3K_4}{2M_s}\sin^2\theta\,\sin4\varphi+\frac{\mu_0}{2}M_s\left(N_y-N_x\right)\sin2\varphi\right]^2\cos^2\theta\right\} \tag{2}$$

where φ_H and θ_H are the angles of the external magnetic field of strength H_0. This resonance equation allows for calculating or fitting the uniform mode's resonances (aligned and unaligned ones).

Micromagnetic Simulations: Micromagnetic simulations have been performed using a GPU-accelerated in-house developed finite element micromagnetic code, the successor of the TetraMag.[42,43] The material parameters in the simulations were chosen such to mimic the ideal single crystal Fe material parameters, namely saturation magnetization

M_s = 1710 kA m^{-1}, exchange stiffness A = 2.1 pJ m^{-1} and cubic anisotropy K_4 = 46.8 kJ m^{-3}. The simulations used free boundary conditions, i.e., no pinning at the edges or surfaces. The ferromagnetic resonance simulations for Fe rods with different length were done similarly to the experimental measurements. For a fixed external mw-frequency field the static magnetic field was swept from high fields to low fields. The resonance fields were determined by plotting the remanence of the magnetization in the direction of the mw-field versus the applied static

**ADVANCED
SCIENCE NEWS**
www.advancedsciencenews.com

**NANO · MICRO
small**
www.small-journal.com

magnetic field. The effect of the misalignment was also studied between the anisotropy easy axis and Fe nanowire axis on the evolution of the angular dependence of the resonance fields.

Conflict of Interest

The authors declare no conflict of interest.

[1] O. G. Schmidt, K. Eberl, *Nature* **2001**, *410*, 168.
[2] F. Balhorn, S. Mansfeld, A. Krohn, J. Topp, W. Hansen, D. Heitmann, S. Mendach, *Phys. Rev. Lett.* **2010**, *104*, 037205.
[3] M. Ying, A. P. Bonifas, N. Lu, Y. Su, R. Li, H. Cheng, A. Ameen, Y. Huang, J. A. Rogers, *Nanotechnology* **2012**, *23*, 344004.
[4] D. Karnaushenko, D. Makarov, C. Yan, R. Streubel, O. G. Schmidt, *Adv. Mater.* **2012**, *24*, 4518.
[5] K. Nielsch, F. J. Castaño, S. Matthias, W. Lee, C. A. Ross, *Adv. Eng. Mater.* **2005**, *7*, 217.
[6] M. Vázquez, *Magnetic Nano- and Microwires: Design, Synthesis, Properties and Applications*, Elsevier, Cambridge **2015**.
[7] D. F. Emerich, C. G. Thanos, *Expert Opin. Biol. Ther.* **2003**, *3*, 655.
[8] S. J. Son, J. Reichel, B. He, M. Schuchman, S. B. Lee, *J. Am. Chem. Soc.* **2005**, *127*, 7316.
[9] ITRS2.0, Beyond CMS, www.itrs2.net (accessed: October 2015).
[10] C. N. R. Rao, R. Sen, B. C. Satishkumar, A. Govindaraj, *Chem. Commun.* **1998**, *0*, 1525.
[11] N. Grobert, W. K. Hsu, Y. Q. Zhu, J. P. Hare, H. W. Kroto, D. R. M. Walton, M. Terrones, H. Terrones, P. Redlich, M. Rühle, R. Escudero, F. Morales, *Appl. Phys. Lett.* **1999**, *75*, 3363.
[12] T. Mühl, D. Elefant, A. Graff, R. Kozhuharova, A. Leonhardt, I. Mönch, M. Ritschel, P. Simon, S. Groudeva-Zotova, C. M. Schneider, *J. Appl. Phys.* **2003**, *93*, 7894.
[13] R. Kozhuharova, M. Ritschel, D. Elefant, A. Graff, A. Leonhardt, I. Mönch, T. Mühl, C. M. Schneider, *J. Mater. Sci.: Mater. Electron.* **2003**, *14*, 789.
[14] D. Golberg, M. Mitome, C. Müller, C. Tang, A. Leonhardt, Y. Bando, *Acta Mater.* **2006**, *54*, 2567.
[15] K. Lipert, S. Bahr, F. Wolny, P. Atkinson, U. Weißker, T. Mühl, O. G. Schmidt, B. Büchner, R. Klingeler, *Appl. Phys. Lett.* **2010**, *97*, 212503.
[16] P. Banerjee, F. Wolny, D. V. Pelekhov, M. R. Herman, K. C. Fong, U. Weissker, T. Mühl, Y. Obukhov, A. Leonhardt, B. Büchner, P. C. Hammel, *Appl. Phys. Lett.* **2010**, *96*, 252505.
[17] C. F. Reiche, J. Körner, B. Büchner, T. Mühl, *Nanotechnology* **2015**, *26*, 335501.
[18] T. Schwarz, R. Wölbing, C. F. Reiche, B. Müller, M. J. Martinez-Pérez, T. Mühl, B. Büchner, R. Kleiner, D. Koelle, *Phys. Rev. Appl.* **2015**, *3*, 044011.
[19] M. U. Lutz, U. Weissker, F. Wolny, C. Müller, M. Löffler, T. Mühl, A. Leonhardt, B. Büchner, R. Klingeler, *J. Phys.: Conf. Ser.* **2010**, *200*, 072062.
[20] F. Wolny, T. Mühl, U. Weissker, K. Lipert, J. Schumann, A. Leonhardt, B. Büchner, *Nanotechnology* **2010**, *21*, 435501.
[21] S. Vock, F. Wolny, T. Mühl, R. Kaltofen, L. Schultz, B. Büchner, C. Hassel, J. Lindner, V. Neu, *Appl. Phys. Lett.* **2010**, *97*, 252505.
[22] T. Mühl, J. Körner, S. Philippi, C. F. Reiche, A. Leonhardt, B. Büchner, *Appl. Phys. Lett.* **2012**, *101*, 112401.
[23] C. F. Reiche, S. Vock, V. Neu, L. Schultz, B. Büchner, T. Mühl, *New J. Phys.* **2015**, *17*, 013014.
[24] A. Banholzer, R. Narkowicz, C. Hassel, R. Meckenstock, S. Stienen, O. Posth, D. Suter, M. Farle, J. Lindner, *Nanotechnology* **2011**, *22*, 295713.
[25] R. Narkowicz, D. Suter, I. Niemeyer, *Rev. Sci. Instrum.* **2008**, *79*, 084702.
[26] R. Narkowicz, D. Suter, R. Stonies, *J. Magn. Reson.* **2005**, *175*, 275.
[27] T. Sebastian, K. Schultheiss, B. Obry, B. Hillebrands, H. Schultheiss, *Front. Phys.* **2015**, *3*, 35.
[28] K. Zakeri, I. Barsukov, N. K. Utochkina, F. M. Romer, J. Lindner, R. Meckenstock, U. van Horsten, H. Wende, W. Keune, M. Farle, S. S. Kalarickal, K. Lenz, Z. Frait, *Phys. Rev. B* **2007**, *76*, 214421.
[29] A. Leonhardt, M. Ritschel, D. Elefant, N. Mattern, K. Biedermann, S. Hampel, C. Müller, T. Gemming, B. Büchner, *J. Appl. Phys.* **2005**, *98*, 074315.
[30] S. Hampel, A. Leonhardt, D. Selbmann, K. Biedermann, D. Elefant, C. Müller, T. Gemming, B. Büchner, *Carbon* **2006**, *44*, 2316.
[31] U. Weissker, S. Hampel, A. Leonhardt, B. Büchner, *Materials* **2010**, *3*, 4387.
[32] F. S. Boi, S. Maugeri, J. Guo, M. Lan, S. Wang, J. Wen, G. Mountjoy, M. Baxendale, G. Nevill, R. M. Wilson, Y. He, S. Zhang, G. Xiang, *Appl. Phys. Lett.* **2014**, *105*, 243108.
[33] Z. Frait, D. Fraitová, *J. Magn. Magn. Mater.* **1980**, *15–18*, 1081.
[34] G. A. Prinz, G. T. Rado, J. J. Krebs, *J. Appl. Phys.* **1982**, *53*, 2087.
[35] J. J. Krebs, F. J. Rachford, P. Lubitz, G. A. Prinz, *J. Appl. Phys.* **1982**, *53*, 8058.
[36] B. K. Kuanr, R. E. Camley, Z. Celinski, *J. Appl. Phys.* **2004**, *95*, 6610.
[37] J. R. Fermin, A. Azevedo, F. M. de Aguiar, B. Li, S. M. Rezende, *J. Appl. Phys.* **1999**, *85*, 7316.
[38] C. Schöppner, K. Wagner, S. Stienen, R. Meckenstock, M. Farle, R. Narkowicz, D. Suter, J. Lindner, *J. Appl. Phys.* **2014**, *116*, 033913.
[39] L. Baselgia, M. Warden, F. Waldner, S. L. Hutton, J. E. Drumheller, Y. Q. He, P. E. Wigen, M. Marysko, *Phys. Rev. B* **1988**, *38*, 2237.
[40] A. Aharoni, *J. Appl. Phys.* **1998**, *83*, 3432.
[41] J. A. Osborn, *Phys. Rev.* **1945**, *67*, 351.
[42] R. Hertel, in *Handbook of Magnetism and Advanced Magnetic Materials* (Eds: H. Kronmüller, S. S. P. Parkin), John Wiley & Sons, New York **2007**, pp. 1003–1020.
[43] A. Kakay, E. Westphal, R. Hertel, *IEEE Trans. Magn.* **2010**, *46*, 2303.
[44] K. Nielsch, R. B. Wehrspohn, J. Barthel, J. Kirschner, S. F. Fischer, H. Kronmüller, T. Schweinböck, D. Weiss, U. Gösele, *J. Magn. Magn. Mater.* **2002**, *249*, 234.